Rapid response of the East Asian trough to Tibetan Plateau snow cover

Wenkai Li[1], Bo Qiu[2, 3]*, Weidong Guo[3, 4], Pang-chi Hsu[1]

[1]Key Laboratory of Meteorological Disaster, Ministry of Education (KLME)/Joint International Research Laboratory of Climate and Environment Change (ILCEC)/Collaborative Innovation Center on Forecast and Evaluation of Meteorological Disasters (CIC-FEMD), Nanjing University of Information Science & Technology, Nanjing, China

[2]Jiangsu Provincial Key Laboratory of Geographic Information Science and Technology, International Institute for Earth System Sciences, Nanjing University, Nanjing, China

[3]School of Atmospheric Sciences, Nanjing University, 210023 Nanjing, China

[4]Joint International Research Laboratory of Atmospheric and Earth System Sciences, Nanjing University, 210023 Nanjing, China.

Revised for *International Journal of Climatology*

(SHORT COMMUNICATIONS)

April, 2020

*Corresponding author: Bo Qiu.

E-mail: qiubo@nju.edu.cn.

KEYWORDS: Tibetan Plateau snow cover; subseasonal variations; East Asian trough; East Asian winter monsoon

FUNDING INFORMATION: National Key Research and Development Program of China, Grant/Award Number: 2018YFC1505804; Natural Science Foundation of China, Grant/Award Number: 41905074; Natural Science Foundation of Jiangsu Province, Grant/Award Number: BK20190782

Abstract

Tibetan Plateau snow cover (TPSC) has subseasonal variations and rapidly influences the atmosphere. In this study, we present the rapid response of the East Asian trough (EAT) within a week to subseasonal variations in TPSC during the boreal winter. Using snow cover analysis obtained from the daily interactive multisensor snow and ice mapping system and the ERA-Interim reanalysis, a considerable relationship between TPSC and 500-hPa geopotential height anomalies over the downstream EAT region is found. Significant negative (positive) 500-hPa geopotential height anomalies originating from the Tibetan Plateau and moving into the EAT region appear within a week following anomalous positive (negative) TPSC events, which lead to changes in EAT strength. Thus, a significantly enhanced (reduced) intensity of the EAT occurs approximately 5–6 days after increased (decreased) TPSC. Numerical experiments confirm the causality of this relationship. Further analysis of the quasi-geostrophic geopotential height tendency equations in numerical experiments indicates that such EAT variations result from anomalous thermal advection from the Tibetan Plateau forced by TPSC.

KEYWORDS: Tibetan Plateau snow cover; subseasonal variations; East Asian trough; East Asian winter monsoon

1 | INTRODUCTION

The Tibetan Plateau, known as the “third pole”, is the highest plateau in the world. Its large and complex topography directly influences atmospheric circulations (Bolin 1950; Yeh 1950; Park et al., 2012; Chen and Bordoni 2014). The orographic forcing by the Tibetan Plateau provides a preferred location for the lee vortex and lee trough (e.g., Luo et al., 1985; Egger and Hoinka 2008; Wang and Tan 2014). In addition to the

orographic effects, the thermal forcing by the Tibetan Plateau strongly affects the climate system over East Asia and beyond (Yanai and Wu, 2006; Wu et al., 2007; Liu et al., 2007; Wang et al., 2014; Yang et al., 2014; Yao et al., 2019).

Snow cover, characterized by high-albedo characteristics, acts as an important lower boundary condition for the atmosphere (Hahn and Shukla, 1976; Barnett et al., 1988; Wu and Kirtman, 2007; Zhang et al., 2017; Jia et al. 2018). The Tibetan Plateau has much more snow cover than other regions at the same latitude due to its high elevation and cold temperature (Xu et al., 2017). The Tibetan Plateau snow cover (TPSC) and its variations exert substantial influences on the weather, climate and ecosystem of the Tibetan Plateau and its surrounding areas (You et al., 2020). In most of the literature, TPSC is generally considered as an atmospheric indicator at interannual (e.g., Wu and Qian, 2003; Lin and Wu, 2011; Xiao and Duan, 2016; Wang et al., 2017; Lyu et al., 2018; Wang et al., 2018; Qian et al., 2019; Qiu et al., 2019; Yuan et al., 2019) and decadal time scales (e.g., Zhao and Moore, 2004; Zhang et al., 2004; Wu et al., 2012; Si and Ding, 2013); other studies have examined the long-term trends of TPSC (e.g., Zhao and Moore, 2006; Zhao et al., 2007).

Snow cover can vary rapidly within a season over discontinuous or sporadic permafrost zones (Wang et al., 2015; Li et al., 2019; Suriano and Leathers, 2018; Song et al., 2019; Song and Wu, 2019). Understanding the rapid variations in snow cover is important for short- and medium-range weather forecasting applications (Clark and Serreze, 2000; Orsolini et al., 2019). Notably, TPSC is distinctly shallow, patchy and frequently of short duration (Qin et al., 2006). Such unique characteristics may lead to fast variations in TPSC within a seasonal period (Li et al., 2016, 2019; Song et al., 2019).

The fast variations in TPSC are dominant signals within a season; they could exert impacts on atmospheric variability over Asia (Li et al., 2018).

The East Asian trough (EAT), characterized by the strongest negative deviation from the zonal mean over East Asia, is one of the most distinct zonally asymmetric circulation features and is closely associated with the East Asian winter monsoon (Zhang et al., 1997; Wang et al., 2009; Song et al., 2016). With variations ranging from synoptic to interannual time scales, the EAT has been recognized as a major atmospheric circulation feature influencing the weather and climate (Chen et al., 2005; Wang et al., 2009; Huang et al., 2012; Chen et al., 2014; Song et al., 2016; Song and Wu, 2018; Sen et al., 2019). Due to the considerable impact of the EAT on weather and climate, understanding the sources of EAT variability is of practical and scientific importance. The EAT is excited by the thermal contrast between the cold Eurasian continent and the warm Pacific Ocean. The mechanism for EAT variations has been suggested to be linked with atmospheric internal variabilities such as Rossby waves and synoptic transient eddies (Wang et al., 2009; Leung and Zhou, 2016; Song et al., 2016), teleconnections such as the North Atlantic Oscillation (Qiao and Feng, 2016) and the Northern Hemisphere Annular Mode (Lu et al., 2016). Sea surface temperature also exerts influences on the EAT (Leung et al., 2017; Feng et al., 2018). However, the effects of lower boundary conditions over the land surface on EAT variations are still not well understood.

Most of the previous studies focused on the climatic effects of TPSC at time scales longer than seasons, and our understanding of the rapid response of the atmosphere to subseasonal TPSC variations is still less complete and requires further study. Recent studies have also shown that better snow cover initialization improves subseasonal and

seasonal forecasts/simulations (Jeong et al., 2013; Orsolini et al., 2013; Senan et al., 2016; Lin et al., 2016; Kolstad 2017), implying that snow cover is a potential indicator for forecasts at shorter time scales. Li et al. (2018) found that the anomalous TPSC rapidly influences subsequent downstream upper-level (300-hPa) atmospheric circulation, with a focus on the East Asia upper-level westerly jet stream. However, how the subseasonal variability in TPSC influences middle-level atmospheric circulation is not clear. In addition, since the EAT plays a key role in the Asian winter monsoon system, how and to what extent the subseasonal variability in TPSC could influence the strength of the EAT is also an open but valuable issue. Therefore, the present study aims to increase our knowledge of the effects of fast subseasonal TPSC variability on the middle-level regional atmosphere, as well as the short-term EAT variations modulated by external forcing.

2 | DATA AND METHODOLOGY

2.1 | Data

Two publicly available datasets are used in this study. (1) Daily snow cover data at 24-km resolution are obtained from the interactive multisensor snow and ice mapping system (IMS) snow cover analysis (Helfrich et al., 2007). The IMS analysis over the Tibetan Plateau corresponds well with ground-based measurements and can capture the general subseasonal variability of TPSC (Yang et al., 2015; Li et al., 2018). (2) The reanalysis of daily averaged geopotential height at 500 hPa (H500) with a horizontal resolution of 0.5° × 0.5° is obtained from the ERA-Interim archive (Dee et al., 2011). To remove the annual cycle and interannual to decadal variability, a 120-day high-pass filter

is applied for all of the variables discussed in this study, except for climatology in Figure 2a. This study spans 22 winters (from November 1997 to February 2019). Each winter comprises 120 days from November 1 to February 28 of the following year.

2.2 | Composite

This study investigates observed features of TPSC influences on the EAT through a composite analysis. The extreme anomalous TPSC events are selected based on the following criteria. First, to measure the regional variability in TPSC, a TPSC index for the entire Tibetan Plateau is defined; this index represents the percentage of snow-covered area across the Tibetan Plateau. The grid points on the Tibetan Plateau are defined as points at elevations greater than 3,000 meters and within 25–43°N and 65–105°E. The Tibetan Plateau contains 7658 grid points in the IMS analysis. The TPSC index for the entire Tibetan Plateau is calculated from the IMS analysis and defined as TPSC index = $\frac{1}{n}\sum_{i=1}^{n} x_i \times 100\%$, where x is the IMS analysis over the Tibetan Plateau, n is the total grid points in analysis. If one grid point is covered by snow, $x = 1$; otherwise, $x = 0$. The unit of TPSC index is %. Then, extreme anomalous TPSC events are selected according to the TPSC index. The TPSC index must be greater than 0.5 (less than −0.5) of its standard deviation during winter for 6 or more consecutive days. Among the 6 or more consecutive days, the day on which the TPSC index is maximum (minimum) is considered the "start day" of this extreme positive (negative) TPSC event. The numbers of positive and negative TPSC events for the composite are 50 and 68, respectively. The composites of these positive (negative) event samples were made based on their "start day" as well as the days that lag the "start day". Here, the composites were derived by simply averaging variables during these event samples.

The simultaneous composites of the TPSC for positive and negative events are presented in Figure 1a and 1b, respectively. These two spatial patterns are quite similar but out of phase. The composites show anomalous TPSC mainly over the central and eastern Tibetan Plateau. To make the results concise, we focus on the differences in TPSC between positive and negative TPSC events (Figure 1c). The snow anomaly signal shows a decreasing tendency and persists up to approximately 5 days (Supplementary Figure S1). In Section 3, the differences the EAT between the composites of positive and negative TPSC events, which are related to differences in TPSC shown in Figure 1c, are studied.

2.3 | Numerical experiments

Numerical experiments were performed using the Advanced Weather Research and Forecasting Model (version 3.9.1). See Supplementary Methods for the model domain and parameterization schemes. Two ensemble experiments are carried out, including positive anomalous TPSC experiments (ExpPOS) and negative anomalous TPSC experiments (ExpNEG). The initial lower boundary condition TPSC is modified based on the IMS analysis. Simultaneous composites of the daily TPSC from the IMS analysis between extreme positive and negative TPSC events (Figure 1c) are treated as anomalies. The climatological wintertime TPSC plus half of the anomalies determine the initial forcing for ExpPOS, whereas the initial forcing for ExpNEG is obtained by the climatological TPSC minus half of the anomalies. The only difference at the initial time step of the model is the snow cover conditions over the Tibetan Plateau for ExpPOS and ExpNEG. The first simulated 24 hours are considered as a spin-up period, and the outputs during this period are excluded from the analysis.

The relation between snow cover and the atmosphere is a two-way coupling connection (Henderson et al., 2018). This study focus only on the TPSC-forced atmospheric response. To eliminate the impacts of atmospheric variability embedded in the initial conditions, we carried out several runs for each experiment with different initial dates and conducted an ensemble mean. Both ExpPOS and ExpNEG contain 12 members with different initial times. We use the 1st, 11th, and 21st days in each month from November 2013 to February 2014 as the initial dates. Since the initial date can be considered random, the internal atmospheric variability in the initial time step can be largely smoothed out after the ensemble average is applied. Using the ensemble means of each member with different initiation times can remove the synoptic variability of the atmosphere but retain the effect of changes in TPSC. A comparison between the ensemble means of ExpPOS and ExpNEG can efficiently reveal the TPSC-forced atmospheric responses. The ensemble technique here is similar to the method used by Vinoj et al. (2014).

2.4 | Geopotential height tendency equation

To elucidate the physical processes contributing to the variations in the EAT, the quasi-geostrophic geopotential height tendency equation is analyzed. The equation is

$$\underset{①}{\left[\nabla^2 + \frac{\partial}{\partial p}\left(\frac{f^2}{\sigma}\frac{\partial}{\partial p}\right)\right]\frac{\partial \Phi}{\partial t}} = \underset{②}{-f\boldsymbol{V}_g \cdot \nabla\left(\frac{1}{f}\nabla^2\Phi + f\right)} \underset{③}{-\frac{\partial}{\partial p}\left[-\frac{f^2}{\sigma}\boldsymbol{V}_g \cdot \nabla\left(-\frac{\partial \Phi}{\partial p}\right)\right]} \underset{④}{-\frac{f^2 R_d}{\sigma c_p}\frac{\partial}{\partial p}\left(\frac{J}{p}\right)}, \quad (1)$$

where Φ is the geopotential height, t is the time, ∇^2 is the Laplacian operator, p is the pressure, f is the Coriolis parameter, σ is the static stability, $\boldsymbol{V}_g$ is the geostrophic

wind vector, R_d is the gas constant of dry air, c_p is the specific heat of dry air at constant volume and J is the diabatic heating rate. Term 1 can be approximated as:

$$\left(\nabla^2 + \frac{f^2}{\sigma}\frac{\partial^2}{\partial p^2}\right)\frac{\partial \Phi}{\partial t} \propto -\frac{\partial \Phi}{\partial t}, \quad (2)$$

where the $\propto$ symbol means "proportional to", i.e., that Term 1 is proportional to $-\partial\Phi/\partial t$. Therefore, when the right-hand side of (1) is positive, $\partial\Phi/\partial t$ is negative, implying a local decrease in the geopotential height with time on a given isobaric surface, and vice versa. Terms 2–4 are the differential vorticity advection term, the differential thermal advection term, and the differential diabatic heating term, respectively, which contribute to Term 1.

3 | OBSERVED FEATURES OF TPSC INFLUENCES ON THE EAT

The EAT is characterized by an elongated area of relatively low H500 compared with the zonal mean over East Asia. Figure 2a shows the winter climatology of H500. The yellow line in Figure 2a indicates the EAT axis, which is the minimum point of H500 over East Asia. The climatology of the EAT axis appears near the Sea of Okhotsk and extends to the Japanese archipelago and the East China Sea. To examine the subseasonal variations in the EAT, an empirical orthogonal function (EOF) analysis is performed on the 120-day high-pass filtered H500 over 25–55°N and 110–160°E. The first leading EOF mode is shown in Figure 2b and explains 30.9% of the total variance. The first EOF mode basically bears a mono-sign pattern with the maximum loading centered over the Sea of Japan and near the EAT axis region, which contributes to the variations in the EAT strength. The spatial distribution of this first EOF mode indicates that the daily variations in H500 near the EAT axis are most dominant over East Asia. To describe such a primary feature of regional variation in H500 over the EAT region, we define an EAT index by

weighted averaging the anomalous H500 over the EAT core region (30–50°N and 120–150°E; magenta box in Figure 2a). The EAT core region covers the climatology of the EAT axis, as well as the dominant center of variation in H500 revealed by the first EOF mode. Note that a negative (positive) anomalous EAT index represents an enhanced (a reduced) intensity of the EAT.

To analyze the connection between TPSC and H500, lagged composite analysis of 120-day high-pass filtered H500 anomalies is performed for extreme TPSC cases. The averaged differences between the positive and negative TPSC events were regarded as composites here. The composites of lagged H500 anomalies with respect to TPSC are shown in Figure 3 and are related to the TPSC anomalies shown in Figure 1c. The TPSC and the spatial distribution of lagged H500 anomalies are strongly related over East Asia. The negative anomalous H500 appears over the Tibetan Plateau at a 1–2 day lag from the start day of an extreme TPSC event (Figure 3a). Then, the negative anomalies of H500 move eastward and reach the EAT region (Figure 3b) at lags of 3–4 days. The center of negative values of H500 is collocated with the EAT core region (i.e., climatological EAT axis) at lags of 5–6 days (Figure 3c). Then, the negative anomalies of H500 continue to propagate eastward, weaken and move out of the EAT region (Figure 3d). To make the results concise, here we focus on the averaged differences of H500 anomalies between the positive and negative TPSC events. This is based on the fact that the anomalous patterns of H500 associated with positive and negative TPSC events are similar but out of phase. See Supplementary Figures S2–S3 for details.

During the propagating journey of H500 anomalies, the strength of EAT varies correspondingly (Figure 4). Lagged composites are calculated for the EAT index and are presented as dark bars in Figure 4 (the EAT index lags TPSC). The EAT index becomes

negative at lags of 3–6 days, consistent with the period when negative H500 anomalies prevail over the EAT region. At lags of 5–6 days, the EAT reaches its maximum intensity. We also obtain similar results based on the singular value decomposition method (Supplementary Figure S4).

4 | PHYSICAL PROCESSES

The above composite analysis with respect to TPSC show that significant negative (positive) H500 anomalies in East Asia are found within a week following positive (negative) TPSC events. H500 anomalies move eastward into the EAT region at lags of 3–6 days. To further understand the mechanisms, we conduct a set of model experiments along with diagnostic analyses.

The difference between ExpPOS and ExpNEG is considered to represent the response or the sensitivity of the atmosphere to increased TPSC, while decreased TPSC leads to a response with the opposite sign of the difference. Figure 5 shows the difference in H500 between ExpPOS and ExpNEG. The signal of the H500 response (negative values) first develops over the eastern Tibetan Plateau at 1–2 days, lagging the initial date of the model (Figure 5a). Then, the H500 response propagates eastward toward the Japanese archipelago and reaches the EAT region at lags of 3–4 days (Figure 5b). The negative values of the H500 response continue to expand eastward and further develop over the EAT region at lags of 5–6 days (Figure 5c). Thereafter, the H500 anomalies propagate farther eastward and weaken at lags of 7–8 days (Figure 5d). Such structures and propagation of the H500 response reveal a general whole life cycle of response to TPSC anomalous events. Along with the propagation of H500 anomalies, there are corresponding EAT responses. The EAT index shows a delayed response to TPSC

(Figure 4). The negative values of differences in the EAT index between ExpPOS and ExpNEG increase (i.e., strengthened EAT) at lags of 1–6 days. The strength of the EAT tends toward the highest response values at lags of 5–6 days. Thereafter, the EAT response decreases.

The response of H500 in the numerical experiments is similar to that in the composites but with some differences. This is because the relation between TPSC and the atmosphere is a two-way coupling connection in real cases, while the numerical experiments focus only on the TPSC-forced response. The composites contain signals not only from the TPSC-forced response but also from the internal atmospheric variability contributing to the TPSC variability. Signals of H500 anomalies over the Tibetan Plateau, which contribute to TPSC variability but are not produced by TPSC, will be contained in composites for anomalous TPSC events. However, these H500 anomalies are excluded in numerical experiments according to the design of numerical experiments.

The quasi-geostrophic geopotential height tendency equation is analyzed to elucidate the physical processes contributing to the variations in the EAT. The response of the geopotential tendency budget at 500 hPa to TPSC at lags of 3–6 days in the numerical experiments over the EAT core region is shown in Figure 6. The difference in Term 1 between ExpPOS and ExpNEG is positive, indicating responses of negative geopotential height tendency at lags of 3–6 days. This result is consistent with the strengthened EAT index response at lags of 3–6 days (Figure 4). Term 3 contributes largely to the changes in H500 (Term 1), while Terms 2 and 4 have relatively small values. The results indicate that the advection of vertically differential temperature anomalies is the key process responsible for the variations in the EAT strength.

The response of temperature and its advection anomalies in the downstream EAT region could be attributable to the temperature anomalies over the Tibetan Plateau induced by snow cover changes because only the TPSC is modified in our model experiments. A decreased response of sensible heat flux is caused by the snow-albedo effect. The response of regional averaged sensible heat flux over the Tibetan Plateau is –55.48 W m^{-2} for the first day in the numerical experiments. Such response rapidly modulates the land surface thermal conditions across the Tibetan Plateau. Note that the 500-hPa pressure level is close to the land surface over the Tibetan Plateau. The TPSC-induced land surface albedo variations and thermal forcing directly influence atmospheric temperature near 500-hPa. Increased (decreased) snow cover leads to an overall enhanced (reduced) cooling effect and decreased (increased) 500-hPa atmospheric temperature. Then, the thermal advection caused by the background of climatological westerly winds influences downstream H500 and EAT responses as revealed by diagnosing Eq. (1).

5 | CONCLUSIONS

Tibetan Plateau snow cover (TPSC) has subseasonal variations and rapidly influences the atmosphere. This study reveals the rapid response of the East Asian trough (EAT) within a week to subseasonal variations in TPSC during the boreal winter. The analyses based on observation reveal the influence of TPSC on the EAT. Significant negative (positive) 500-hPa geopotential height anomalies originate from the Tibetan Plateau and move into the EAT region and strengthen (weaken) the EAT after the occurrence of positive (negative) TPSC events. The maximum impact of TPSC on the EAT occurs at lags of 5–6 days. Numerical experiments confirm the causality of this

relationship. Further analysis of the quasi-geostrophic geopotential height tendency equations in numerical experiments indicates that such EAT variations are results of anomalous thermal advection from the Tibetan Plateau forced by TPSC.

The time scale for the influence of TPSC on the EAT is approximately one week, indicating that TPSC can serve as an indicator of the middle troposphere on the synoptic to medium range, including the EAT. This result also provides an important reference for validating the response of the atmosphere to TPSC in numerical models.

The fast variations in TPSC focused in this work are mainly over the central and eastern Tibetan Plateau (as shown in Figure 1). Note that the western TPSC also exerts significant influences on the atmosphere but on longer timescales due to its longer persistence and memory (e.g., Wu et al., 2012; Xiao et al., 2019). Future studies on the influence of western Tibetan Plateau snow on the EAT at longer timescales are also potentially valuable.

ACKNOWLEDGMENTS

This research is supported by the National Key Research and Development Program of China (2018YFC1505804), Natural Science Foundation of China (41905074), the Natural Science Foundation of Jiangsu Province (BK20190782). This work is also supported by Jiangsu Collaborative Innovation Center for Climate Change. The IMS snow cover data are available at https://nsidc.org/data/G02156/versions/1. The ERA-interim data are available at http://apps.ecmwf.int/datasets/. The WRF source codes can be obtained at http://www2.mmm.ucar.edu/wrf/users/downloads.html. The WRF is driven by the National Centers for Environmental Prediction FNL Operational Model Global Tropospheric Analyses, which are available at https://rda.ucar.edu/datasets/ds083.2/. All figures were produced using the NCAR Command Language (NCL), version 6.6.2, which is free to the public (http://dx.doi.org/10.5065/D6WD3XH5). The authors declare no competing interests.

REFERENCES

Barnett, T. P., Dumenil, L., Schlese, U. and Roeckner, E. (1988) The effect of Eurasian snow cover on global climate. *Science*, 239(4839), 504. https://doi.org/10.1126/science.239.4839.504

Bolin, B. (1950) On the influence of the earth's orography on the general character of the westerlies. *Tellus*, 2(3), 184–195. https://doi.org/10.3402/tellusa.v2i3.8547

Chen, J. and Bordoni, S. (2014) Orographic effects of the Tibetan Plateau on the East Asian summer monsoon: An energetic perspective. *Journal of Climate*, 27(8), 3052–3072. https://doi.org/10.1175/jcli-d-13-00479.1

Chen, S., Chen, X., Wei, K., Chen, W., and Zhou, T. (2014) Vertical tilt structure of East Asian trough and its interannual variation mechanism in boreal winter. *Theoretical and Applied Climatology*, 115(3–4), 667–683. https://doi.org/10.1007/s00704-013-0928-7

Chen, W., Yang, S., and Huang, R. H. (2005) Relationship between stationary planetary wave activity and the East Asian winter monsoon. *Journal of Geophysical Research-Atmospheres*, 110, D14110. https://doi.org/10.1029/2004jd005669

Clark, M. P. and Serreze, M. C. (2000) Effects of variations in east Asian snow cover on modulating atmospheric circulation over the north pacific ocean. *Journal of Climate*, 13(20), 3700–3710. https://doi.org/10.1175/1520-0442(2000)013<3700:eoviea>2.0.co;2

Dee, D. P., Uppala, S. M., Simmons, A. J., Berrisford, P., Poli, P., Kobayashi, S., et al. (2011) The ERA-Interim reanalysis: configuration and performance of the data assimilation system. *Quarterly Journal of the Royal Meteorological Society*, 137(656), 553–597. https://doi.org/10.1002/qj.828

Egger, J. and Hoinka, K.-P. (2008) Mountain torque events at the Tibetan Plateau. *Monthly Weather Review*, 136(2), 389–404. https://doi.org/10.1175/2007mwr2126.1

Feng, G., Zou, M., Qiao, S., Zhi, R., and Gong, Z. (2018) The changing relationship between the December North Atlantic Oscillation and the following February East Asian trough before and after the late 1980s. *Climate Dynamics*, 51(11–12), 4229–4242. https://doi.org/10.1007/s00382-018-4165-8

Hahn, D. G. and Shukla, J. (1976) An apparent relationship between Eurasian snow cover and Indian monsoon rainfall. *Journal of the Atmospheric Sciences*, 33(12), 2461–2462. https://doi.org/10.1175/1520-0469(1976)033<2461:aarbes>2.0.co;2

Helfrich, S. R., McNamara, D., Ramsay, B. H., Baldwin, T., and Kasheta, T. (2007) Enhancements to, and forthcoming developments in the Interactive Multisensor Snow and Ice Mapping System (IMS). *Hydrological Processes*, 21(12), 1576–1586. https://doi.org/10.1002/hyp.6720

Henderson, G. R., Peings, Y., Furtado, J. C. and Kushner, P. J. (2018) Snow–atmosphere coupling in the Northern Hemisphere. *Nature Climate Change*, 8(11), 954–963. https://doi.org/10.1038/s41558-018-0295-6

Huang, R., Chen, J., Wang, L., and Lin, Z. (2012) Characteristics, processes, and causes of the spatio-temporal variabilities of the East Asian monsoon system. *Advances in Atmospheric Sciences*, 29(5), 910–942. https://doi.org/10.1007/s00376-012-2015-x

Jeong, J. H., Linderholm, H. W., Woo, S. H., Folland, C., Kim, B. M., Kim, S. J., and Chen, D. L. (2013) Impacts of snow initialization on subseasonal forecasts of surface air temperature for the cold season. *Journal of Climate*, 26(6), 1956–1972. https://doi.org/10.1175/jcli-d-12-00159.1

Jia, X., Cao, D. R., Ge, J. W. and Wang, M. (2018) Interdecadal change of the impact of Eurasian snow on spring precipitation over southern China. *Journal of Geophysical Research: Atmospheres*, 123(18), 10092–10108. https://doi.org/10.1029/2018jd028612

Kolstad, E. W. (2017) Causal pathways for temperature predictability from snow depth. *Journal of Climate*, 30(23), 9651–9663. https://doi.org/10.1175/jcli-d-17-0280.1

Leung, M. Y.-T., and Zhou, W. (2016) Eddy contributions at multiple timescales to the evolution of persistent anomalous East Asian trough. *Climate Dynamics*, 46(7–8), 2287–2303. https://doi.org/10.1007/s00382-015-2702-2

Leung, M. Y. T., Cheung, H. H. N. and Zhou, W. (2017) Meridional displacement of the East Asian trough and its response to the ENSO forcing. *Climate Dynamics*, 48(1–2), 335–352. https://doi.org/10.1007/s00382-016-3077-8

Li, W., Guo, W., Hsu, P.-C., and Xue, Y. (2016) Influence of the Madden–Julian oscillation on Tibetan Plateau snow cover at the intraseasonal time-scale. *Scientific Reports*, 6, 30456. https://doi.org/10.1038/srep30456

Li, W., Guo, W., Qiu, B., Xue, Y., Hsu, P.-C., and Wei, J. (2018) Influence of Tibetan Plateau snow cover on East Asian atmospheric circulation at medium-range time scales. *Nature Communications*, 9(1), 4243. https://doi.org/10.1038/s41467-018-06762-5

Li, W., Qiu, B., Guo, W., Zhu, Z. and Hsu, P.-C. (2019) Intraseasonal variability of Tibetan Plateau snow cover. *International Journal of Climatology*, 1–16. https://doi.org/10.1002/joc.6407

Lin, H., and Wu, Z. (2011) Contribution of the autumn Tibetan Plateau snow cover to seasonal prediction of North American winter temperature. *Journal of Climate*, 24(11), 2801–2813. https://doi.org/10.1175/2010jcli3889.1

Lin, P., Wei, J., Yang, Z. -L., Zhang, Y., and Zhang, K. (2016) Snow data assimilation-constrained land initialization improves seasonal temperature prediction. *Geophysical Research Letters*, 43, 11423–11432. https://doi.org/10.1002/2016GL070966

Liu, Y., Hoskins, B., and Blackburn, M. (2007) Impact of Tibetan orography and heating on the summer flow over Asia. Journal of the Meteorological *Society of Japan. Ser. II*, 85B, 1–19. https://doi.org/10.2151/jmsj.85B.1

Lu, C., Zhou, B., and Ding, Y. (2016) Decadal variation of the Northern Hemisphere Annular Mode and its influence on the East Asian trough. *Journal of Meteorological Research*, 30(4), 584–597. https://doi.org/10.1007/s13351-016-5105-3

Luo, M., Zhu, B. and Zhang, X. (1985) The dynamic effect of the Tibetan Plateau on the formation of zonal type circulation over East Asia. *Advances in Atmospheric Sciences*, 2(2), 158–166. https://doi.org/10.1007/bf03179748

Lyu, M., Wen, M. and Wu, Z. (2018) Possible contribution of the inter-annual Tibetan Plateau snow cover variation to the Madden-Julian oscillation convection variability. *International Journal of Climatology*, 38(10), 3787–3800. https://doi.org/10.1002/joc.5533

Orsolini, Y. J., Senan, R., Balsamo, G., Doblas-Reyes, F. J., Vitart, F., Weisheimer, A., et al. (2013) Impact of snow initialization on sub-seasonal forecasts. *Climate Dynamics*, 41(7–8), 1969–1982. https://doi.org/10.1007/s00382-013-1782-0

Orsolini, Y.J., Wegmann, M., Dutra, E., Liu, B., Balsamo, G., Yang, K., de Rosnay, P., Zhu, C., Wang, W., Senan, R. and Arduini, G. (2019) Evaluation of snow depth and snow cover over the Tibetan Plateau in global reanalyses using in situ and satellite remote sensing observations. *The Cryosphere*, 13(8), 2221–2239. https://doi.org/10.5194/tc-13-2221-2019

Park, H.-S., Chiang, J. C. H. and Bordoni, S. (2012) The Mechanical Impact of the Tibetan Plateau on the Seasonal Evolution of the South Asian Monsoon. *Journal of Climate*, 25(7), 2394–2407. https://doi.org/10.1175/jcli-d-11-00281.1

Qian, Q., Jia, X. and Wu, R. (2019) Changes in the Impact of the Autumn Tibetan Plateau Snow Cover on the Winter Temperature Over North America in the mid-1990s. *Journal of Geophysical Research-Atmospheres*, 124(19), 10321–10343. https://doi.org/10.1029/2019jd030245

Qiao, S., and Feng, G. (2016) Impact of the December North Atlantic Oscillation on the following February East Asian trough. *Journal of Geophysical Research-Atmospheres*, 121, 10074–10088. https://doi.org/10.1002/2016jd025007

Qin, D. H., Liu, S. Y. and Li, P. J. (2006) Snow cover distribution, variability, and response to climate change in western China. *Journal of Climate*, 19(9), 1820–1833. https://doi.org/10.1175/jcli3694.1

Qiu, B., Li, W., Wang, X., Shang, L., Song, C., Guo, W., and Zhang, Y. (2019) Satellite-observed solar-induced chlorophyll fluorescence reveals higher sensitivity of alpine ecosystems to snow cover on the Tibetan Plateau. *Agricultural and Forest Meteorology*, 271, 126–134. https://doi.org/10.1016/j.agrformet.2019.02.045

Sen, O. L., Ezber, Y., and Bozkurt, D. (2019) Euro-Mediterranean climate variability in boreal winter: a potential role of the East Asian trough. *Climate Dynamics*, 52(11), 7071–7084. https://doi.org/10.1007/s00382-018-4573-9

Senan, R., Orsolini, Y. J., Weisheimer, A., Vitart, F., Balsamo, G., Stockdale, T. N., et al. (2016) Impact of springtime Himalayan-Tibetan Plateau snowpack on the onset of the Indian summer monsoon in coupled seasonal forecasts. *Climate Dynamics*, 47(9–10), 2709–2725. https://doi.org/10.1007/s00382-016-2993-y

Si, D., and Ding, Y. (2013) Decadal change in the correlation pattern between the Tibetan Plateau winter snow and the East Asian summer precipitation during 1979–2011. *Journal of Climate*, 26(19), 7622–7634. https://doi.org/10.1175/jcli-d-12-00587.1

Song, L., Wang, L., Chen, W., and Zhang, Y. (2016) Intraseasonal variation of the strength of the East Asian trough and its climatic impacts in boreal winter. *Journal of Climate*, 29(7), 2557–2577. https://doi.org/10.1175/jcli-d-14-00834.1

Song, L., and Wu, R. (2018) Comparison of intraseasonal East Asian winter cold temperature anomalies in positive and negative phases of the Arctic Oscillation. *Journal of Geophysical Research: Atmospheres*, 123(16), 8518–8537. https://doi.org/10.1029/2018jd028343

Song, L. and Wu, R. (2019) Intraseasonal snow cover variations over western Siberia and associated atmospheric processes. *Journal of Geophysical Research: Atmospheres*, 124(16), 8994–9010. https://doi.org/10.1029/2019jd030479

Song, L., Wu, R. G. and An, L. (2019) Different sources of 10-to 30-day intraseasonal variations of autumn snow over western and eastern Tibetan Plateau. *Geophysical Research Letters*, 46(15), 9118–9125. https://doi.org/10.1029/2019gl083852

Suriano, Z. J. and Leathers, D. J. (2018) Great lakes basin snow-cover ablation and synoptic-scale circulation. *Journal of Applied Meteorology and Climatology*, 57(7), 1497–1510. https://doi.org/10.1175/jamc-d-17-0297.1

Vinoj, V., Rasch, P. J., Wang, H., Yoon, J.-H., Ma, P.-L., Landu, K. and Singh, B. (2014) Short-term modulation of Indian summer monsoon rainfall by West Asian dust. *Nature Geoscience*, 7, 308–313. https://doi.org/10.1038/ngeo2107

Wang, C., Yang, K., Li, Y., Wu, D., and Bo, Y. (2017) Impacts of spatiotemporal anomalies of Tibetan Plateau snow cover on summer precipitation in Eastern China. *Journal of Climate*, 30(3), 885–903. https://doi.org/10.1175/jcli-d-16-0041.1

Wang, L., Chen, W., Zhou, W., and Huang, R. (2009) Interannual variations of East Asian trough axis at 500 hPa and its association with the East Asian winter monsoon pathway. *Journal of Climate*, 22(3), 600–614. https://doi.org/10.1175/2008jcli2295.1

Wang, Q.-W. and Tan, Z.-M. (2014) Multi-scale topographic control of southwest vortex formation in Tibetan Plateau region in an idealized simulation. *Journal of Geophysical Research: Atmospheres*, 119(20), 11543–11561. https://doi.org/10.1002/2014jd021898

Wang, T., Peng, S., Ottle, C. and Ciais, P. (2015) Spring snow cover deficit controlled by intraseasonal variability of the surface energy fluxes. *Environmental Research Letters*, 10, 024018. https://doi.org/10.1088/1748-9326/10/2/024018

Wang, Z., Duan, A., and Wu, G. (2014) Time-lagged impact of spring sensible heat over the Tibetan Plateau on the summer rainfall anomaly in East China: case studies using the WRF model. *Climate Dynamics*, 42(11), 2885–2898. https://doi.org/10.1007/s00382-013-1800-2

Wang, Z., Wu, R., Chen, S., Huang, G., Liu, G. and Zhu, L. (2018) Influence of western Tibetan Plateau summer snow cover on East Asian summer rainfall. *Journal of Geophysical Research-Atmospheres*, 123(5), 2371–2386. https://doi.org/10.1002/2017jd028016

Wu, G., Liu, Y., Wang, T., Wan, R., Liu, X., Li, W., et al. (2007) The influence of mechanical and thermal forcing by the Tibetan Plateau on Asian climate. *Journal of Hydrometeorology*, 8(4), 770–789. https://doi.org/10.1175/jhm609.1

Wu, R. and Kirtman, B. P. (2007) Observed relationship of spring and summer East Asian rainfall with winter and spring Eurasian snow. *Journal of Climate*, 20(7), 1285–1304. https://doi.org/10.1175/jcli4068.1

Wu, T., and Qian, Z. (2003) The relation between the Tibetan winter snow and the Asian summer monsoon and rainfall: An observational investigation. *Journal of Climate*, 16(12), 2038–2051. https://doi.org/10.1175/1520-0442(2003)016<2038:trbttw>2.0.co;2

Wu, Z., Jiang, Z., Li, J., Zhong, S., and Wang, L. (2012) Possible association of the western Tibetan Plateau snow cover with the decadal to interdecadal variations of northern China heatwave frequency. *Climate Dynamics*, 39(9–10), 2393–2402. https://doi.org/10.1007/s00382-012-1439-4

Xiao, Z., and Duan, A. (2016) Impacts of Tibetan Plateau snow cover on the interannual variability of the East Asian summer monsoon. *Journal of Climate*, 29(23), 8495–8514. https://doi.org/10.1175/jcli-d-16-0029.1

Xiao, Z., Duan, A. and Wang, Z. (2019) Atmospheric heat sinks over the western Tibetan Plateau associated with snow depth in late spring. *International Journal of Climatology*, 39(13), 5170–5180. https://doi.org/10.1002/joc.6133

Xu, W., Ma, L., Ma, M., Zhang, H., and Yuan, W. (2017) Spatial-temporal variability of snow cover and depth in the Qinghai-Tibetan Plateau. *Journal of Climate*, 30(4), 1521–1533. https://doi.org/10.1175/jcli-d-15-0732.1

Yanai, M., and Wu, G. (2006) Effects of the Tibetan Plateau. In B. Wang (Ed.), The Asian Monsoon (pp. 513–549). Berlin, Heidelberg: Springer Berlin Heidelberg.

Yang, J., Jiang, L., Ménard, C. B., Luojus, K., Lemmetyinen, J., and Pulliainen, J. (2015) Evaluation of snow products over the Tibetan Plateau. *Hydrological Processes*, 29(15), 3247–3260. https://doi.org/10.1002/hyp.10427

Yang, K., Wu, H., Qin, J., Lin, C., Tang, W., and Chen, Y. (2014) Recent climate changes over the Tibetan Plateau and their impacts on energy and water cycle: A review. *Global and Planetary Change*, 112, 79–91. https://doi.org/10.1016/j.gloplacha.2013.12.001

Yao, T., Xue, Y., Chen, D., Chen, F., Thompson, L., Cui, P., et al. (2019) Recent Third Pole's rapid warming accompanies cryospheric melt and water cycle intensification and interactions between monsoon and environment: Multidisciplinary approach with observations, modeling, and analysis. *Bulletin of the American Meteorological Society*, 100(3), 423–444. https://doi.org/10.1175/bams-d-17-0057.1

Yeh, T.-C. (1950) The circulation of the high troposphere over China in the winter of 1945–46. *Tellus*, 2(3), 173–183. https://doi.org/10.3402/tellusa.v2i3.8548

You, Q., Wu, T., Shen, L., Pepin, N., Zhang, L., Jiang, Z., Wu, Z., Kang, S. and AghaKouchak, A. (2020) Review of snow cover variation over the Tibetan Plateau and its influence on the broad climate system. *Earth-Science Reviews*, 201, 103043. https://doi.org/10.1016/j.earscirev.2019.103043

Yuan, C., Li, W., Guan, Z. and Yamagata, T. (2019) Impacts of April snow cover extent over Tibetan Plateau and the central Eurasia on Indian Ocean Dipole. *International Journal of Climatology*, 39(3), 1756–1767. https://doi.org/10.1002/joc.5888

Zhang, R., Zhang, R., and Zuo, Z. (2017) Impact of Eurasian spring snow decrement on East Asian summer precipitation. *Journal of Climate*, 30(9), 3421–3437. https://doi.org/10.1175/jcli-d-16-0214.1

Zhang, Y., Sperber, K. R., and Boyle, J. S. (1997) Climatology and interannual variation of the East Asian winter monsoon: Results from the 1979-95 NCEP/NCAR reanalysis. *Monthly Weather Review*, 125(10), 2605–2619. https://doi.org/10.1175/1520-0493(1997)125<2605:caivot>2.0.co;2

Zhang, Y., Li, T., and Wang, B. (2004) Decadal change of the spring snow depth over the Tibetan Plateau: The associated circulation and influence on the East Asian summer monsoon. *Journal of Climate*, 17(14), 2780–2793. https://doi.org/10.1175/1520-0442(2004)017<2780:dcotss>2.0.co;2

Zhao, H., and Moore, G. W. K. (2004) On the relationship between Tibetan snow cover, the Tibetan plateau monsoon and the Indian summer monsoon. *Geophysical Research Letters*, 31, L14204. https://doi.org/10.1029/2004gl020040

Zhao, H. and Moore, G. W. K. (2006) Reduction in Himalayan snow accumulation and weakening of the trade winds over the Pacific since the 1840s. *Geophysical Research Letters*, 33, L17709. https://doi.org/10.1029/2006gl027339

Zhao, P., Zhou, Z., and Liu, J. (2007) Variability of Tibetan spring snow and its associations with the hemispheric extratropical circulation and East Asian summer monsoon rainfall: An observational investigation. *Journal of Climate*, 20(15), 3942–3955. https://doi.org/10.1175/jcli4205.1

Figure captions

FIGURE 1 The simultaneous composites of the daily anomalous Tibetan Plateau snow-cover probabilities for (**a**) positive events and (**b**) negative events. (**c**) The difference between (**a**) and (**b**). The unit is %. The black contour marks the regions of the Tibetan Plateau with elevations higher than 3000 m.

FIGURE 2 (**a**) Climatology of the wintertime 500-hPa geopotential height (H500; shading). The unit is m. The magenta rectangle shows the subdomain of the East Asian trough (EAT) core region (30–50°N, 120–150°E). The yellow line shows the trough axis in the climatology of wintertime H500. (**b**) The first leading mode of the empirical

orthogonal function (EOF) based on daily H500 anomalies. This mode explains 30.9% of the total variance of H500 anomalies.

FIGURE 3 Composites of 500-hPa geopotential height (H500) anomalies with respect to the start day of Tibetan Plateau snow cover (TPSC) events in observations at lags of (**a**) 1−2 days, (**b**) 3−4 days, (**c**) 5−6 days, and (**d**) 7−8 days. The composites show the differences in averaged H500 anomalies between positive and negative TPSC events. The unit is m. The purple contour marks the regions of the Tibetan Plateau with elevations higher than 3000 m. Stippled regions mark composites with significance at the 99% level (two-tailed Student's *t* test).

FIGURE 4 Response of the East Asian trough (EAT) index to Tibetan Plateau snow cover (TPSC). The dark bars show the differences between averaged EAT index anomalies in positive and negative TPSC events from observations. The light bars show the difference in the EAT index between ExpPOS and ExpNEG from numerical experiments, which represent the response of the EAT index to increased TPSC. The *x*-axis represents the number of days lagging the start of TPSC events or the model initial date. The unit is m.

FIGURE 5 Responses of 500-hPa geopotential height (H500) to Tibetan Plateau snow cover (TPSC) in numerical experiments at lags of (**a**) 1−2 days, (**b**) 3−4 days, (**c**) 5−6 days, and (**d**) 7−8 days from the initial date of the model integration. Shadings show differences between ExpPOS and ExpNEG, which represent the response of the atmosphere to increased TPSC. The unit is m. The purple contour marks the regions of the Tibetan Plateau with elevations higher than 3000 m.

FIGURE 6 The response of the geopotential tendency budget at 500 hPa to the Tibetan Plateau snow cover at lags of 3–6 days in the numerical experiments over the East Asian trough core region (30–50°N, 120–150°E). Terms on the *x*-axis from left to right are the geopotential tendency (Term 1), the differential vorticity advection (Term 2), the differential thermal advection (Term 3), and the differential diabatic heating (Term 4). The unit is $1e^{-14}$ s^{-3}. Note that Term 1 is inversely proportional to geopotential tendency. See equation (1) for further details.

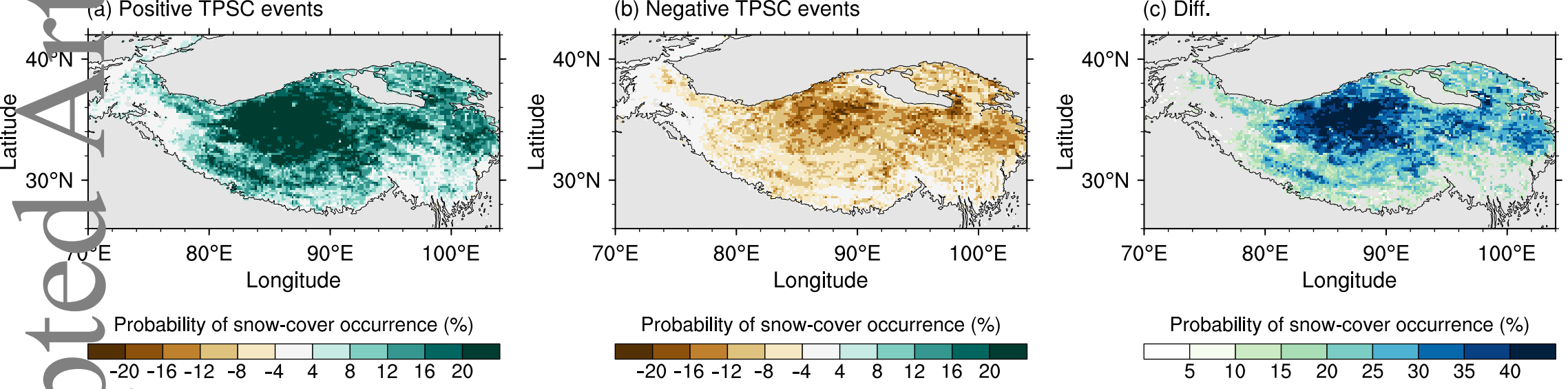

FIGURE 1 The simultaneous composites of the daily anomalous Tibetan Plateau snow-cover probabilities for (**a**) positive events and (**b**) negative events. (**c**) The difference between (**a**) and (**b**). The unit is %. The black contour marks the regions of the Tibetan Plateau with elevations higher than 3000 m.

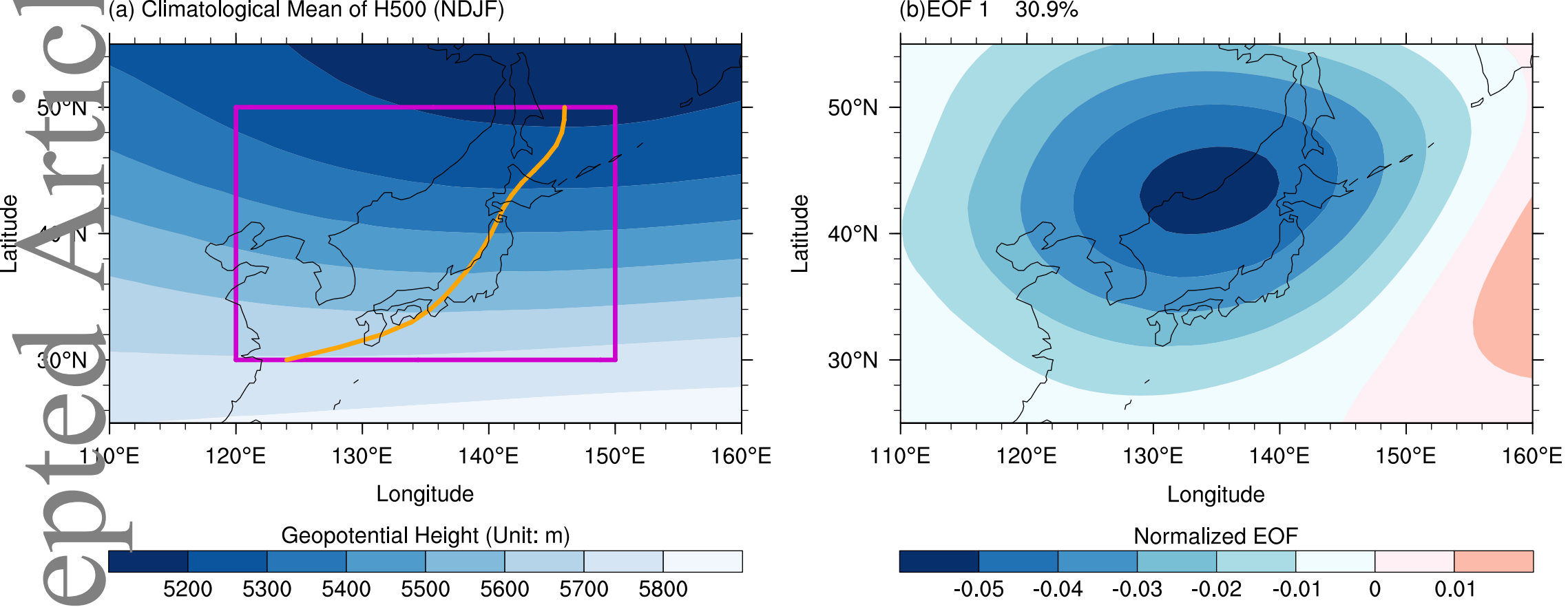

FIGURE 2 (**a**) Climatology of the wintertime 500-hPa geopotential height (H500; shading). The unit is m. The magenta rectangle shows the subdomain of the East Asian trough (EAT) core region (30–50°N, 120–150°E). The yellow line shows the trough axis in the climatology of wintertime H500. (**b**) The first leading mode of the empirical orthogonal function (EOF) based on daily H500 anomalies. This mode explains 30.9% of the total variance of H500 anomalies.

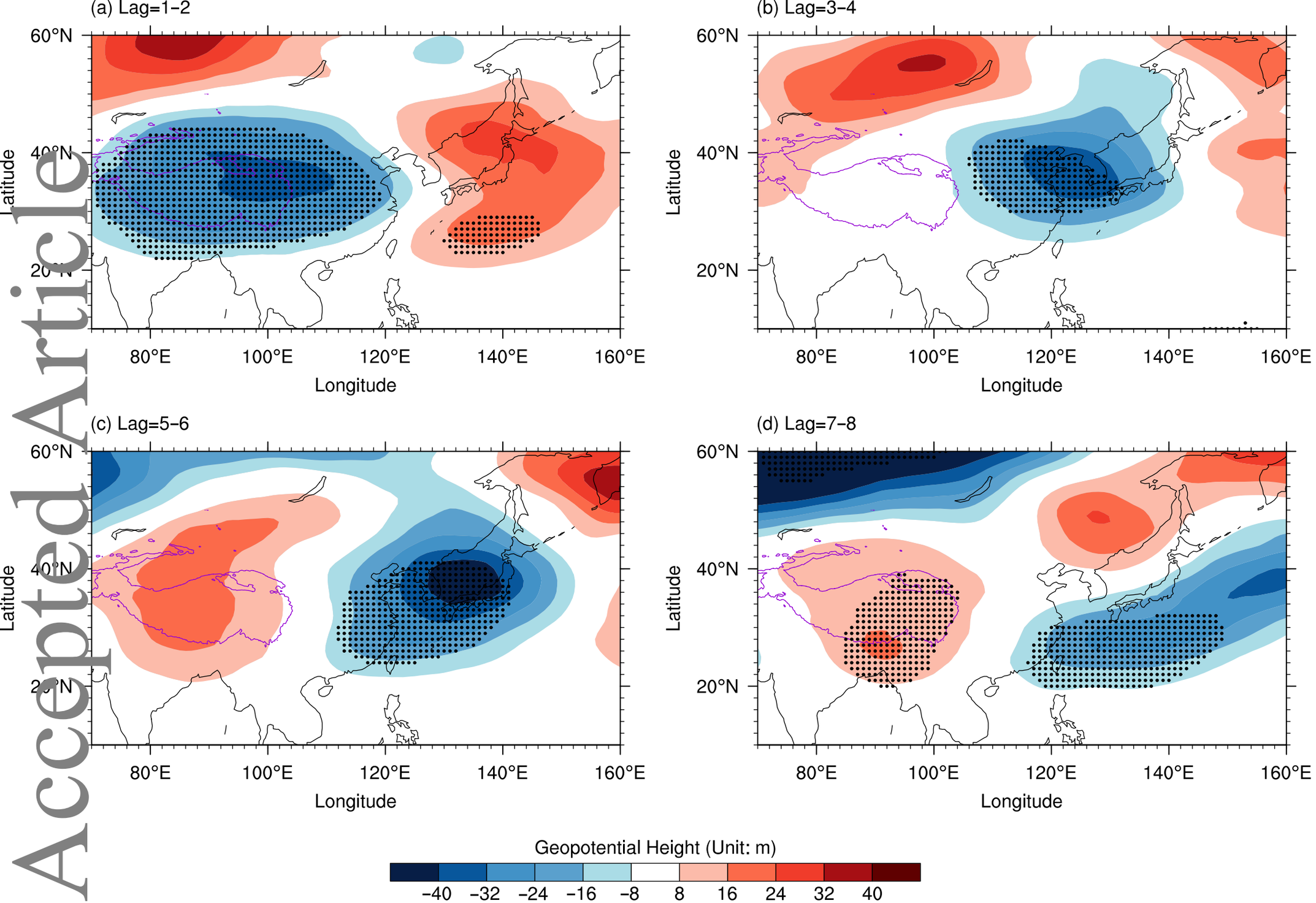

FIGURE 3 Composites of 500-hPa geopotential height (H500) anomalies with respect to the start day of Tibetan Plateau snow cover (TPSC) events in observations at lags of (**a**) 1−2 days, (**b**) 3−4 days, (**c**) 5−6 days, and (**d**) 7−8 days. The composites show the differences in averaged H500 anomalies between positive and negative TPSC events. The unit is m. The purple contour marks the regions of the Tibetan Plateau with elevations higher than 3000 m. Stippled regions mark composites with significance at the 99% level (two-tailed Student's *t* test).

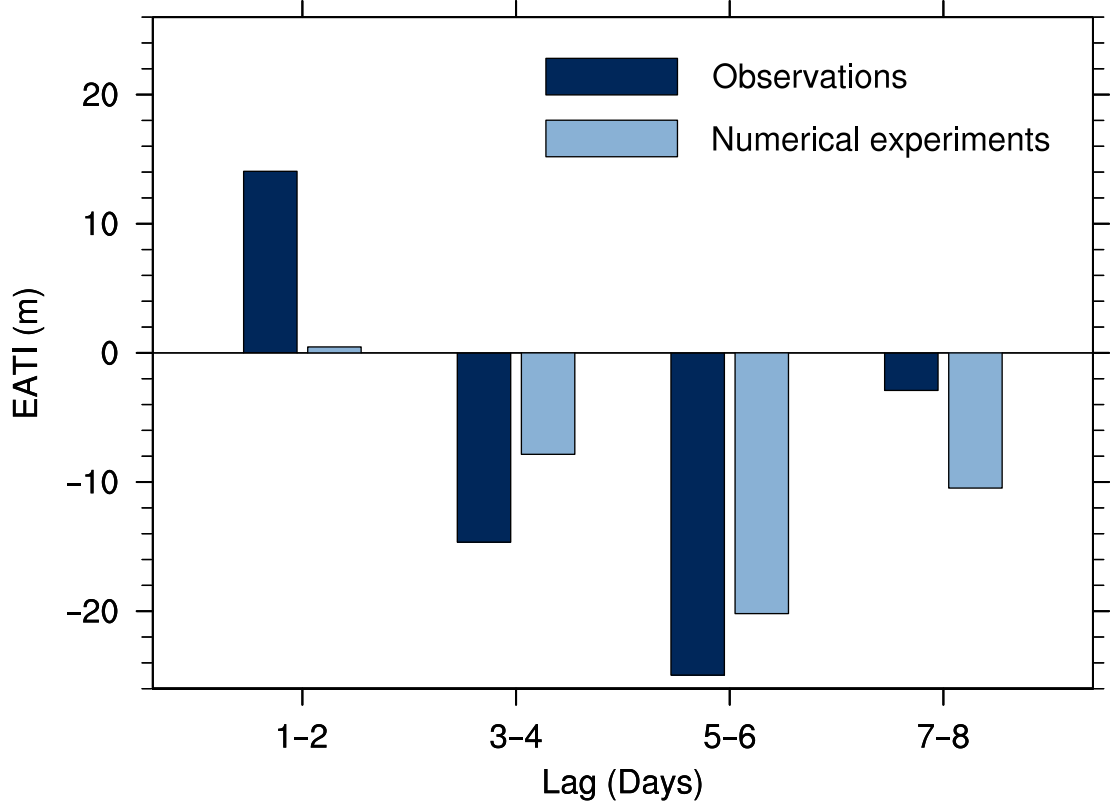

FIGURE 4 Response of the East Asian trough (EAT) index to Tibetan Plateau snow cover (TPSC). The dark bars show the differences between averaged EAT index anomalies in positive and negative TPSC events from observations. The light bars show the difference in the EAT index between ExpPOS and ExpNEG from numerical experiments, which represent the response of the EAT index to increased TPSC. The x-axis represents the number of days lagging the start of TPSC events or the model initial date. The unit is m.

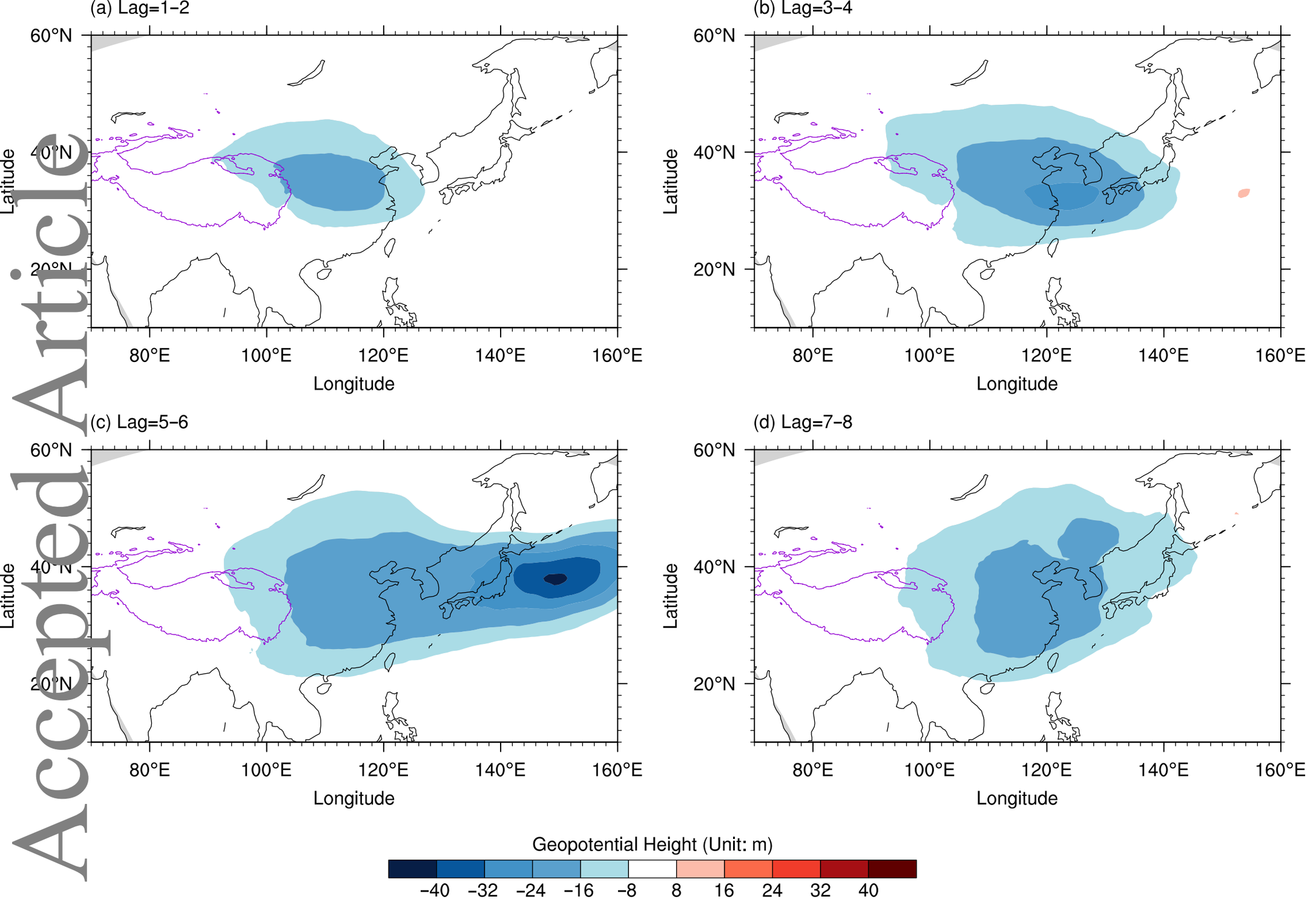

FIGURE 5 Responses of 500-hPa geopotential height (H500) to Tibetan Plateau snow cover (TPSC) in numerical experiments at lags of (**a**) 1−2 days, (**b**) 3−4 days, (**c**) 5−6 days, and (**d**) 7−8 days from the initial date of the model integration. Shadings show differences between ExpPOS and ExpNEG, which represent the response of the atmosphere to increased TPSC. The unit is m. The purple contour marks the regions of the Tibetan Plateau with elevations higher

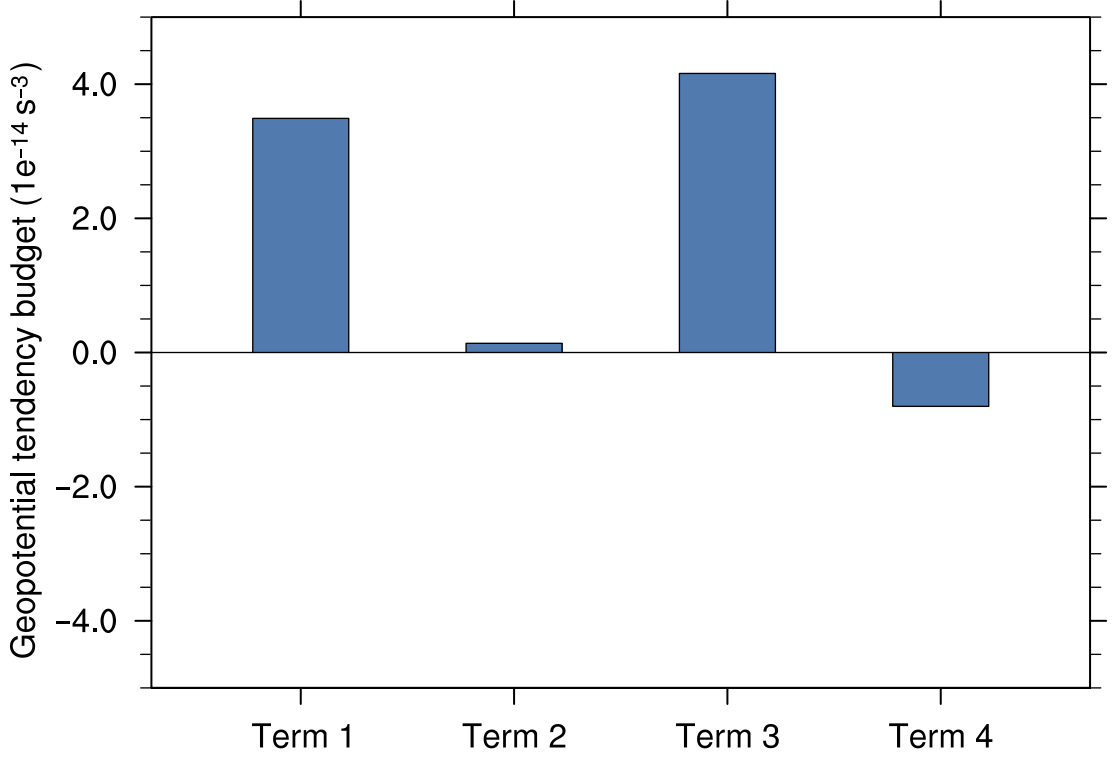

FIGURE 6 The response of the geopotential tendency budget at 500 hPa to the Tibetan Plateau snow cover at lags of 3–6 days in the numerical experiments over the East Asian trough core region (30–50°N, 120–150°E). Terms on the *x*-axis from left to right are the geopotential tendency (Term 1), the differential vorticity advection (Term 2), the differential thermal advection (Term 3), and the differential diabatic heating (Term 4). The unit is 1e^{-14} s^{-3}. Note that Term 1 is inversely proportional to geopotential tendency. See equation (1) for further details.